Kinetic quantitative analysis reveals the suppression of Sup35NM amyloid fibril nucleation by liquid–liquid phase separation.

Mao Fukuyama[a,b], Suguru Nishinami[c], Yoko Maruyama[a], Taiki Ozawa[a], Shunsuke Tomita[d], Yumiko Ohhashi[e], Motohiro Kasuya[f], Masao Gen[a], Eri Chatani[e], Kentaro Shiraki[c], and Akihide Hibara[a,g]

[a]Institute of Multidisciplinary Research for Advanced Materials, Tohoku University, 2-1-1, Katahira, Sendai, Miyagi 980-8577, Japan.

[b]Organization for Advanced Studies, Tohoku University, 2-1-1 Katahira, Sendai, Miyagi 980-8577, Japan.

[c]Faculty of Pure and Applied Sciences, University of Tsukuba,1-1-1, Tennoudai, Tsukuba, Ibaraki 305-8573, Japan.

[d]Health and Medical Research Institute, The National Institute of Advanced Industrial Science and Technology, 1-1-1 Higashi, Tsukuba, Ibaraki 305-8566, Japan.

[e]Graduate School of Science Kobe University, 1-1, Rokkoudaichou, Nada, Kobe, Hyogo 657-8501, Japan.

[f]Faculty of Production Systems Engineering and Sciences Komatsu University, Nu 1-3, Yonchoumemachi, Komatsu, Ishikawa 923-0971, Japan.

[g]Riken, 2-1, Hirosawa, Wako, Saitama 351-0198, Japan.

*Mao Fukuyama and Akihide Hibara. 2-1-1 Katahira, Aokbaku, Sendai, Miyagi, 980-8577, Japan. +81-22-217-5396

Email: maofukuyama@tohoku.ac.jp, hibara@tohoku.ac.jp

Author Contributions: M.F. conceived and designed the research; M.F., N.S., Y.O., E.C., and K.S. designed the experiments; S.N., Y.O., and K.S. prepared proteins; M.F., Y.M., and T.O. acquired and analyzed the experimental data; S.T., M.K., M.G., and A.H. advised the research. The manuscript was prepared by M.F. and edited by all co-authors.

Competing Interest Statement: The authors declare no competing interests.

Classification: Chemistry in PHYSICAL SCIENCE, or Biophysics and Computational Biology in BIOLOGICAL SCIENCE

Keywords: Amyloid nucleation, liquid–liquid phase separation, Sup35, droplets.

This PDF file includes:

Main Text
Figures 1 to 4

Abstract

Amyloid fibril formation is involved in various human diseases, such as amyotrophic lateral sclerosis and Parkinson’s disease. Many amyloidogenic proteins undergo liquid–liquid phase

separation (LLPS), forming liquid-like droplets of condensed proteins. Although these droplets represent potential amyloid nucleation sites, the kinetics of amyloid nucleation in droplets is poorly understood owing to the lack of quantitative analytical methods. This study aimed to develop a measurement method for the determination of amyloid droplet nucleation rate based on image analysis. The prion determinant domain of the yeast prion protein Sup35 (Sup35NM), a known model protein of prion diseases, was used for demonstration. Droplets (1–20 μm in size) of Sup35NM were fixed in agarose gels, and amyloid nucleation in each droplet was determined by observation with confocal micrographs. Upon comparing the amyloid nucleation rates in the droplets and aqueous solutions, we found a critical concentration (C^*) for Sup35NM: amyloid nucleation was suppressed by LLPS above C^*, whereas it was enhanced below C^*. These results highlight that droplet formation can suppress amyloid nucleation, contrary to conventional hypotheses that profess that amyloid nucleation is enhanced by droplet formation. The proposed quantitative measurement method can provide insights into LLPS's role in amyloidosis-related proteins from pathological perspectives.

Significance Statement

A new image analysis method was proposed to quantitatively describe amyloid nucleation kinetics in protein droplets resulting from LLPS. The nucleation kinetics in Sup35NM droplets were analyzed by two-step nucleation model, similar to the nucleation in aqueous solutions. The nucleation in the droplets was significantly slower than expected, suggesting that droplet formation suppressed protein aggregation, despite protein condensation. This new insight contributes to a further understanding of the relationship between LLPS and the pathology of amyloid-related diseases.

Main Text

Introduction

The formation of protein aggregates, including amyloid fibrils, is a ubiquitous process in nature and is often associated with human diseases, such as amyotrophic lateral sclerosis, Huntington's disease, and Parkinson's disease (1, 2). Typically, these fibrils form an ordered cross-β structure, in which β-strands are stacked perpendicular to the longer axis of each fibril. The formation of amyloid aggregates is described by the nucleation-dependent model, a process that comprises nucleation and elongation of fibrils, which is the same as protein crystallization (3, 4). In this model, nucleation is rare and reversible, whereas elongation irreversibly proceeds once nucleation occurs. The nucleation of amyloid fibrils has been widely investigated because it is a critical process in amyloid generation(5, 6).

Many amyloidogenic proteins, including α-synuclein(7), FUS (8), Tau (9, 10), TDP-43(11), TIA-1 (12), hnRNPA1 (13), and Sup35 (14), undergo liquid–liquid phase separation (LLPS) in the cells, forming small, liquid-like droplets (Figure 1A). During biological LLPS of proteins, a protein-condensed phase (in the form of droplets, $C_{droplet}$) spontaneously appears in the protein-depleted phase (C'), whereas the protein amount (M) is preserved. Intrinsically disordered regions (IDRs), which are commonly contained in amyloidogenic proteins, induce LLPS through weak multivalent intermolecular interactions, such as electrostatic, cation-π, and π - π interactions (15–17).

Because the protein concentration in the droplets formed by LLPS is extremely high (typically 200–300 mg/mL) (18), droplet formation of amyloidogenic proteins is thought to increase the risk of amyloid generation by promoting aggregation in cells (7). Amyloid generation in droplets has been often observed both *in vitro* (8, 12, 13, 19–22) and *in silico* (23). Simulations predict that the nucleation barrier decreases or becomes negligible (as in spinodal decomposition) in such a high

concentration range, according to several nucleation theories (23–26). In contrast to *in vitro*/*in silico*, the enhancement of amyloid formation caused by LLPS has seldom been observed *in vivo*. To our knowledge, amyloid formation enhancement by LLPS in an *in vivo* experiment has only been confirmed for α-synuclein to date (7). Explaining the contradiction in results between *in vivo* and *in vitro/in silico* experiments is crucial for in-depth investigations of amyloidosis pathologies. However, the knowledge of amyloid nucleation kinetics in droplets is still limited owing to the lack of quantitative measurement methods focused on droplets. As physicochemical properties and molecular interactions in droplets are largely different from those in aqueous solutions (27), it is difficult to predict the amyloid nucleation kinetics in droplet by extrapolating that in aqueous solutions.

Here, we propose a quantitative analysis method for amyloid nucleation in droplets based on image analysis to reveal the nucleation kinetics. By counting the droplets where nucleation occurs, the nucleation rate was calculated. We chose the Sup35 NM domain (Sup35NM) as a model protein of prion diseases (28–32) and compared the nucleation kinetics between the droplet and aqueous solution. We found a critical concentration (*C**) of Sup35NM (Figure 1B): amyloid nucleation was suppressed by LLPS above *C** but was enhanced below *C**. This finding provides insights into the effect of LLPS on amyloid formation *in vivo*.

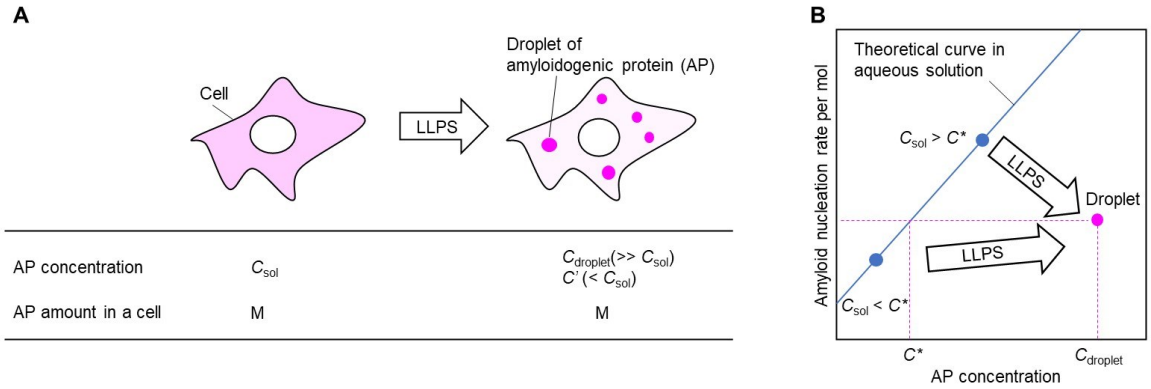

Figure 1. Effect of liquid–liquid phase separation on amyloid nucleation. (A) Schematic images of the amounts and concentrations of amyloidogenic protein (AP) before and after LLPS. The AP concentration increases inside droplets ($C_{droplet}$ >> C_{sol}) and decreases outside droplets (protein-depleted phase C' < C_{sol}), whereas the AP amount in a cell (M) is preserved. (B) A schematic illustration describing the effect of AP concentration on the amyloid nucleation rate. Amyloid nucleation is suppressed by LLPS when C_{sol} > C^*, whereas it is enhanced when C_{sol} < C^*. Details are discussed in Figure 4.

Results

Formation of Sup35NM droplets in agarose gel. For long-term observation of amyloid generation from Sup35NM droplets, we fixed Sup35NM droplets in agarose gel (Figure 2A). The N-terminal domain of Sup35 is a non-charged IDR relating to amyloid formation (29, 33), and the middle (M) domain is a charged IDR that induces pH-dependent droplet formation (14). Sup35NM was mixed with polyethylene glycol (PEG) at pH 6 to induce LLPS (14) gelated with agarose. Spherical assemblies were observed immediately after mixing (Figure 2B). No assemblies were observed in the absence of Sup35NM or PEG (Figure S1). Rhodamine 6G (R6G), a fluorescent dye that typically accumulates in droplets (34), and thioflavin T (ThT), an amyloid indicator, were detected in the spherical assemblies. Analysis of the fluorescence intensities (FIs) of the droplets containing Alpha Fluor 488-conjugated Sup35NM (AF488Sup35NM) indicated that the concentrations of AF488Sup35NM inside and outside of the assemblies were 1160 ± 150 μM

and 18.2 ± 0.3 μM, respectively. The fluidity of Sup35NM in the assemblies was evaluated by fluorescence recovery after photobleaching (FRAP, Figure 2C). The recovery time of fluorescence in AF288Sup35NM assemblies (~11 s) was similar to the reported value in liquid-like Sup35 droplets (~10 s) (14), regardless of agarose addition. This behavior indicated that these assemblies were not gel-like aggregates but liquid-like droplets. Moreover, the FRAP recovery curves were consistent between assemblies and Sup35NM droplets, suggesting that agarose did not affect the motility of Sup35NM droplets.

To investigate the transfer of Sup35NM molecules between droplets, a whole AF488Sup35 droplet was bleached, and its fluorescence recovery was monitored (Droplet 1 in Figure 2D). Fluorescence did not recover for over 1 h, indicating slow molecular exchange between the droplet and solution. The FI of Droplet 2, which was close to that of Droplet 1 (Figure 2D), did not decrease after bleaching Droplet 1, showing limited Sup35NM transfer between droplets.

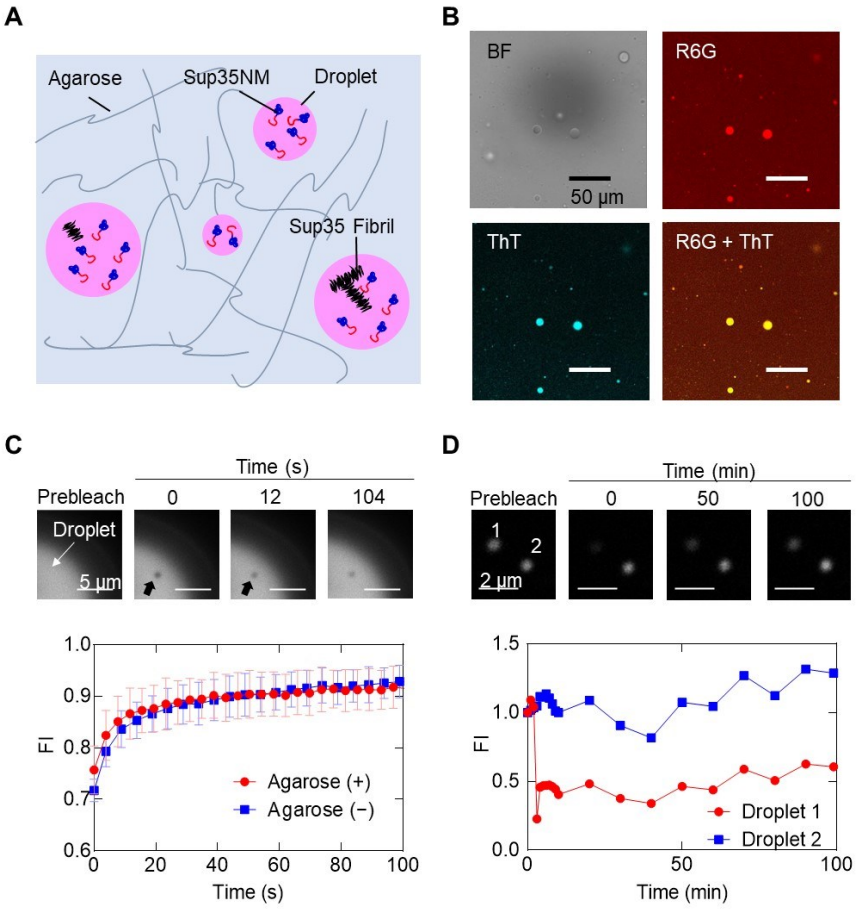

Figure 2. Sup35NM droplets in agarose gel. (A) Schematic illustration of the Sup35NM droplets fixed in agarose gel. Amyloid nucleation in these droplets was investigated. (B) Bright field and fluorescence micrographs. Fluorescence is derived from 20 μM ThT or 5 μM R6G; scale bar, 50 μm. (C) Fluorescence images of AF488Sup35NM droplets during fluorescence recovery after photobleaching (FRAP), with recovery curves. FI indicates the fluorescence intensity of the region of interest (black arrow); scale bar, 5 μm (D) Fluorescence micrographs of AF488Sup35NM droplets during whole FRAP, with recovery curves; scale bar, 2 μm.

Next, we investigated the amyloid formation rates of Sup35NM droplets dispersed in agarose gel by observation with a confocal microscope (Figure 3A). The diameters of the observed droplets were approximately 1–20 μm. The droplets were stable, and the droplet size remained constant for 5.5 h (coefficient of variation, CV = 6%, Figure S2). We calculated the normalized FI of ThT (*F*, Equation 1 in Materials and Methods), which is proportional to ThT concentration, to evaluate amyloid formation. *FI* was uniform at t =1.0 h ($2.0 \times 10^4 \pm 0.4 \times 10^4$) when amyloids had not yet formed (Figure 3B). *F* suddenly increased in some droplets, indicating amyloid formation, but it did not increase in others (Figure 3A and B). These results show that amyloid formation was stochastic in the droplets, indicating the occurrence of amyloid nucleation. After *F* increased, the fibrils extended from the droplets (e.g., 5.5 h in Figure 3A), similar to a previous observation of amyloid formation in droplets *in vitro* (8).

To distinguish between droplets with and without amyloid nucleation, the threshold of *F* ($F_{threshold}$) was determined as 4×10^4 following Equation 2 in Materials and Methods. A total of 300 droplets, with diameters ranging from 2.5 to 8.0 μm, were sorted by size and equipartitioned into four size ranges. The ratio of the number of droplets with nucleation to the total number of droplets ($N_{nucleation}/N_{total}$) was calculated for each size range. $N_{nucleation}/N_{total}$ increased with time and size (Figure 3C). The time evolution of $N_{nucleation}/N_{total}$ was analyzed using the two-step nucleation model, which is a common model to describe amyloid nucleation (Figure 3D) (24, 26, 35–38). This model assumes that the oligomers of amyloidogenic protein formed reversibly from monomers, becoming nuclei in the amyloid (25, 26, 35–38). The time change in $N_{nucleation}/N_{total}$ (Figure 3C) was reproduced based on this model, assuming that the first nucleation event in the droplet can induce a sufficiently high increase in *F* to exceed $F_{threshold}$ (Equation 7). The analyses assuming more than one nucleation are shown in Figure S3. The time constant of Equation 7 ($JV/2t$, Figure 3E) increased with droplet size. By dividing $JV/2t$ by the droplet volume (V) of each size range, the nucleation rate $J/t = k_o k_f {C_{droplet}}^{n_o+n_{conv}}$ $m^{-3}s^{-2}$ (Equation 5 and SI Appendix) was calculated as approximately 10^7 m^{-3} s^{-1} and insensitive to the droplet size (Figure 3F). The analytical results with a different number of size ranges are reported in Figure S5. The reproducibility is shown in Figure S6. The addition of agarose and PEG did not affect the nucleation rate (Figure S7).

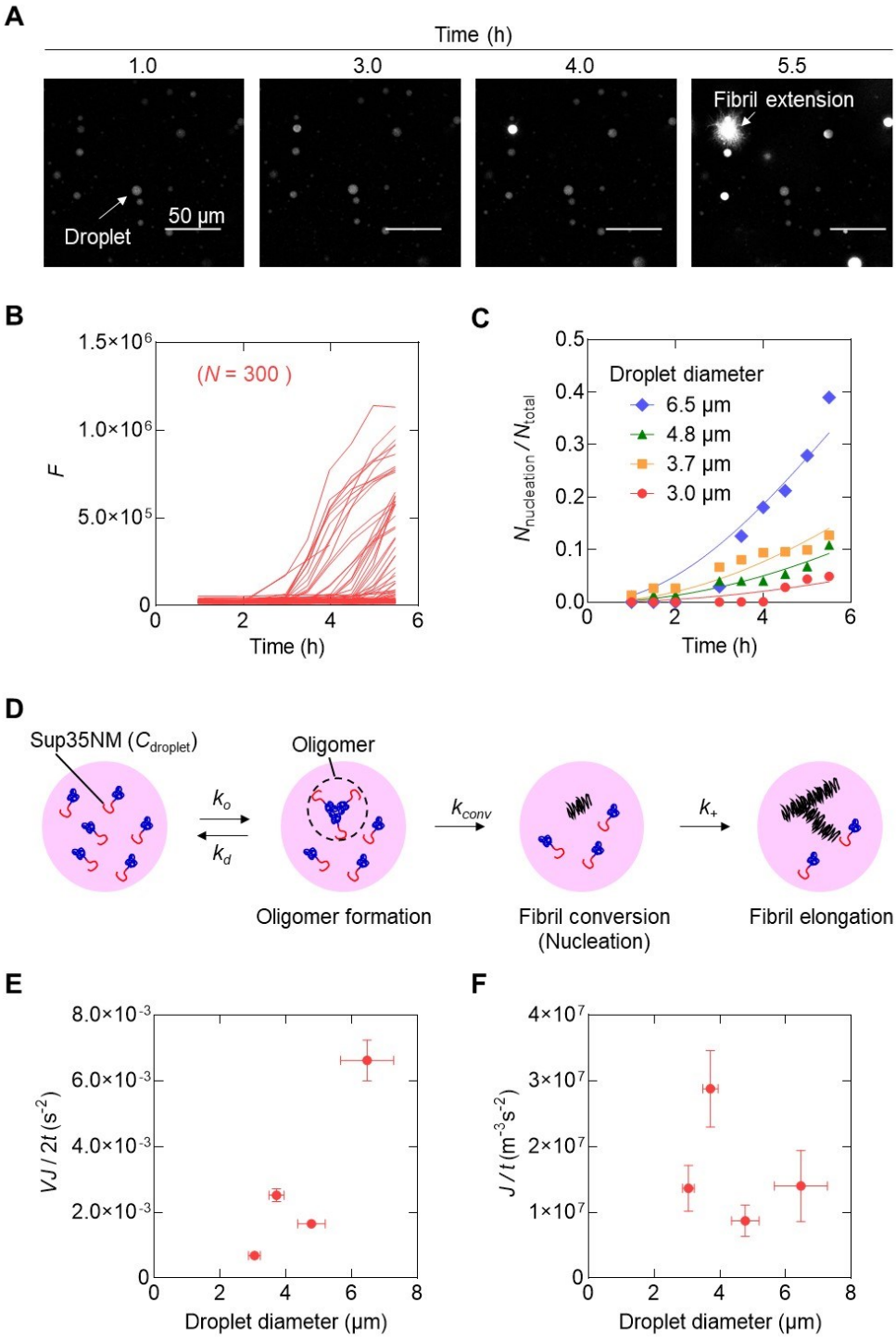

Figure 3. Amyloid formation in Sup35NM droplets. (A) Confocal micrographs of Sup35NM droplets showing fluorescence from ThT. Fluorescence intensity increased with time owing to amyloid formation. (B) Time evolutions of normalized fluorescence intensity (F) of the droplets. (C) Time evolution of the ratio of droplets in which more than one nucleus was generated ($N_{nucleation}/N_{total}$). The curve indicates the fitting based on Equation 6. (D) Schematic illustration of two-step nucleation in a Sup35NM droplet. In the droplet (pink circle), Sup35NM oligomers gradually form. Oligomers

are converted into fibrils at a rate constant of k_{conv}. Amyloid fibrils grow at an elongation rate constant of k_+. (E) Time constant of Equation 7 ($VJ/2t$) versus droplet diameter. The error bars in the x-axis indicate the standard deviations of the droplets. The error bars in the y-axis reflect standard deviations of the fitting in Figure 3C. (F) Nucleation rate (J/t) versus droplet diameter. The error bars in the x-axis indicate the standard deviations of the droplets. The error bars in the y-axis reflect the propagations of standard deviations of VJ/t and the droplet volume, V.

To discuss the effect of LLPS on amyloid nucleation, Sup35NM amyloid nucleation in the droplets was compared with that in an aqueous solution. Here, the ThT FIs of Sup35NM aqueous solutions and droplet suspension were measured in a 384-well plate, using a plate reader. The aqueous solution contained the same matrix as that in the droplet experiment, except PEG. As shown in Figure 4A, the time evolution of ThT FI was faster with the droplets than without droplets, even when the total Sup35NM amount in the well was the same (FI before normalization is shown in Figure S8A). The inverse of the lag time ($1/t_{lag}$) of the ThT FI, which is often used for the semi-quantitative comparison of the amyloid nucleation rate (7, 39), was higher with droplets than in solutions (Figure 4B). These results are conventionally interpretated that droplet formation enhanced amyloid nucleation. However, the comparison of the kinetic parameters of amyloid nucleation (J/t and J_{mol}/t in Figure 4C and D) between the droplets and aqueous solutions showed the opposite tendency: droplet formation suppressed amyloid nucleation. FI was analyzed using the global fit of the secondary nucleation model in Amylofit (5) (Conversion of the rate constants in the secondary nucleation model into those in the two-step nucleation model is explained in SI Appendix). The rate constants and order of amyloid nucleation in the solutions were determined as $k_o k_{conv}$ = 12.8 × 10^5 and $n_o + n_{conv}$ = 3.68, respectively (Figure 4C). Next, we calculated the nucleation rate per mol ($J_{mol} = J/tC = k_o k_{conv} C^{n_o+n_{conv}-1}$ (mol $^{-1}$ s^{-2})), instead of per volume. J_{mol} is essential to compare the risk of amyloid nucleation before and after LLPS because the molecular amount of amyloidogenic protein (AP) in a cell is preserved (Figure 1A). In the experiments using an aqueous solution, J_{mol} increased with an increase in Sup35NM concentration because $n_o+n_{conv} - 1 = 2.68$. Surprisingly, $J_{mol}$was lower in the droplets than in the aqueous solution when Sup35NM concentration in solution (C_{sol}) ≥ C^* ≈ 10 μM. This means that the nucleation was slower in the droplets than in the solution if $C_{sol} \geq C^*$. It should be noted that this tendency can be reproduced by kinetic analysis using Amylofit under several assumptions (Figure S8B and C). The observation of J_{mol} opposes the conclusion from the comparison of t_{lag} (Figure 4B) and the previous simulation work predicting that droplet nucleation would accelerate at higher concentration ranges owing to increasing oligomer size (23, 25, 26). Overall, the present findings highlight that LLPS reduces the risk of amyloid formation of Sup35NM when C_{sol} is higher than C^* ≈ 10 μM.

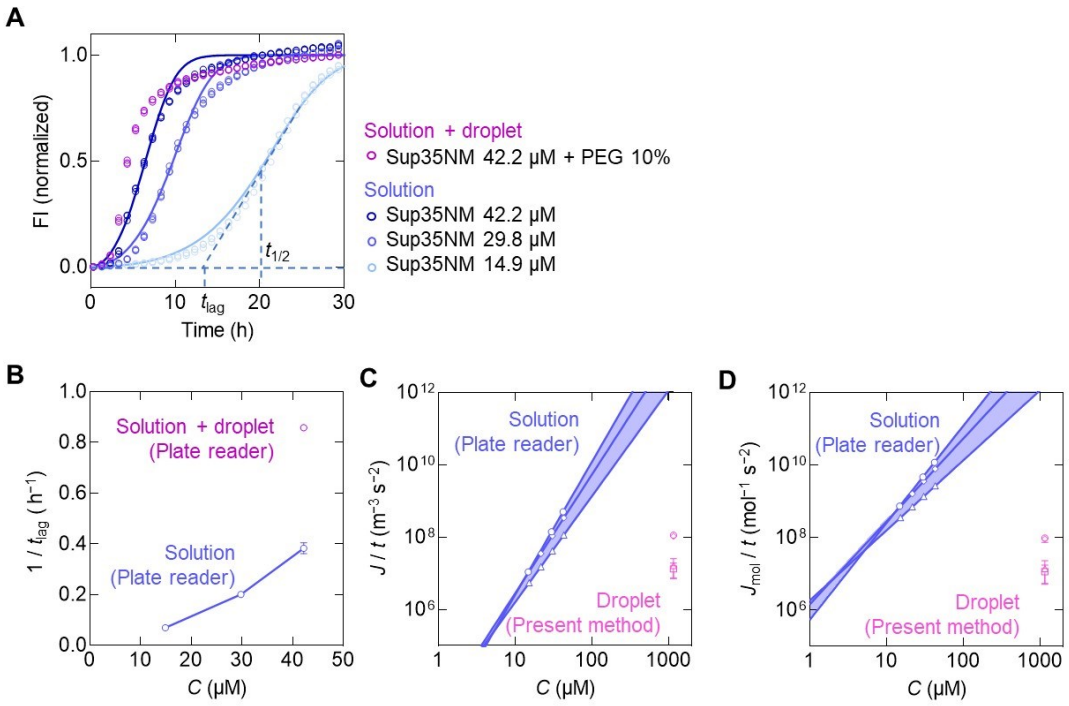

Figure 4. Comparison of the amyloid nucleation rate between droplet and solution. (A) Time evolution of ThT fluorescence intensity (FI) measured using a plate reader (N = 3). (B) Comparison of the inverse of lag time ($1/t_{lag}$). The error bar indicates the standard deviation (SD) of three experiments. (C) Comparison of the amyloid nucleation rate (J/t) in solution measured by a plate reader and droplets measured by the proposed method. The different symbols indicate different series of experiments. The error bars reflect the propagations of SDs of VJ/t and the droplet volume, V. (D) Comparison of the amyloid nucleation rate per mol (J_{mol}/t) in solution measured by a plate reader and droplets measured by the proposed method. The error bars reflect the propagations of SDs of J/t. Higher $1/t_{lag}$, J/t, and J_{mol}/t indicate faster amyloid nucleation.

Discussion

In this study, we quantified amyloid nucleation rates in the droplets of amyloidogenic protein using a developed image analytical method. The results revealed that the nucleation rates in Sup35NM droplets were lower than those in aqueous solutions when $C_{sol} > C^*$ (10 μM). In LLPS conditions achieved by using PEG, the binodal concentration ($C_{binodal}$), which is the same as the concentration of protein-depleted phase C', was 18 μM. Since $C_{binodal} > C^*$, LLPS did not enhance amyloid nucleation but suppressed it. It should be noted that the relationship between C^* and $C_{binodal}$ changed depending on the protein species and LLPS conditions, such as PEG concentrations, pH, and additives. Our findings showed that droplet formation condensed the proteins and could suppress amyloid formation at high protein concentrations, suggesting that droplet formation suppresses unwilling protein aggregation, despite hypotheses predicting the opposite (7, 8, 23, 25). Our proposed quantitative measurement method can enable further discussion of the significance of LLPS for amyloidosis-related proteins from pathological perspectives.

Moreover, our findings indicate that the comparison of the lag time (t_{lag}) (7, 39) with the time evolution of ThT FI, which is conventionally used to evaluate amyloid nucleation rate qualitatively, does not necessarily reflect the intrinsic amyloid nucleation rates. To compare the nucleation rate

between droplets and solutions, a detailed reaction kinetic analysis as performed in this study is needed, even if the total amount of the amyloidogenic protein is the same.

The present method indicated the rate reduction of $J/t = k_o k_{conv} C^{n_o + n_{conv}}$ in the droplets but could not indicate the rate reduction of oligomer formation from monomers ($k_o C^{no}$) and oligomer conversion into fibrils ($k_{conv} C^{n_{conv}}$) separately. Although the mechanism of suppression was not clear, we speculate that the physicochemical properties of the droplets may be involved. For instance, the high viscosity of the droplets (40) reduces the nucleation rate, as is thought to occur in semi-crystalline polymers (41). The stabilization of certain protein structures in the crowding environment (42) of the droplets may reduce amyloid nucleation. The detailed molecular mechanism must be investigated using other analytical methods, such as fluorescence protein–protein interaction analysis. Future investigations on the relationship between droplet size and nucleation will deepen our understanding of amyloid nucleation from droplets.

Materials and Methods

Materials

ThT, sodium dihydrogen phosphate dihydrate ($NaH_2PO_4 \cdot 2H_2O$), PEG, disodium hydrogenphosphate (Na_2HPO_4), sodium hydroxide (NaOH), and R6G were obtained from FUJIFILM Wako Pure Chemical Corporation (Osaka, Japan). Agarose ultra-low gelling temperature and ANS were from Sigma-Aldrich (St. Louis, MO, USA). TrisHCl-buffered saline (TBS, pH 7.4) was obtained from NIPPON GENE (Tokyo, Japan).

Plasmid construction

For the bacterial expression of Sup35NM, pET29b vectors, including a C-terminal 7× histidine-tag, were used. Cysteine addition mutations were introduced at the Sup35NM C-terminal end by site-directed mutagenesis (Takara Bio, Kusatsu, Japan) and confirmed by DNA sequencing.

Expression and purification of Sup35NM protein

Sup35NM was overexpressed in the bacterial strain BL21 (DE3) and purified by nickel-nitrilotriacetic acid histidine-tag affinity chromatography (Thermo Fisher Scientific) fi and cation-exchange chromatography (Cytiva) under denaturing conditions, as described previously (43). Bacteria expressing the target protein were lysed with 6 M guanidine hydrochloride (GdnHCl) and 10 mM TrisHCl (pH 8.0). The soluble fraction was aliquoted onto a nickel column, equilibrated with 8 M urea and 10 mM TrisHCl (pH 8.0), and eluted with 250 mM imidazole. The His-tagged coalescence proteins were aliquoted onto a cation-exchange column and equilibrated with 8 M urea and 10 mM 2-morpholinoethanesulfonic acid buffer (pH 6.0). Then, the target protein and degradants were separated with 1 M NaCl at a 5–20% gradient. Purified Sup35NM was passed through a 300-kDa filter (Sartorius) to remove pre-existing aggregates and was stocked in a solution containing 6 M GdnHCl and 10 mM TrisHCl (pH 8.0) at 4 °C. To purify cysteine mutants, 1 mM DL-dithiothreitol (DTT) was added to the buffer.

Preparation of AF488Sup35

After 2 h of 20 mM Tris (2-carboxyethyl) phosphine hydrochloride treatment, cysteine-adducted Sup35NM was treated with a 10-fold excess volume of Alpha Fluor 488 C5 Maleimide (AAT Bioquest, Sunnyvale, CA, USA) in 6 M GdnHCl at room temperature (20–30 °C) for 2 h. AF488Sup35 was purified via nickel-nitrilotriacetic acid affinity chromatography.

Preparation of Sup35NM droplets in agarose gel

Aqueous solutions of 30% PEG (pH 6, buffered with 3.9 mM phosphate buffer and NaOH), 1 μM ThT, 80 mM phosphate buffer (pH 6), and 4% agarose (melted at 70 °C) were mixed in a microtube at 40 °C. Just after mixing, 3.9 mM or 4.3 mM Sup35NM aqueous solution, containing 6 M GdnHCl and 10 mM TrisHCl buffer (pH 8), was added to the microtube and gently mixed via a micropipette. The sample was transferred to a glass-bottom 384-well plate (Sensoplate™,

Greiner Bio-One GmbH, Kremsmuenster, Austria) and cooled in the refrigerator (4 °C) for 5 min. The composition of the prepared sample was 39 μM Sup35NM, 2% agarose, 10% PEG, 20 μM ThT, 60 mM GdnHCl, 0.1 mM Tris buffer, and 4.3 mM phosphate buffer.

FRAP analysis

AF488Sup35 droplets were prepared following the procedure described for Sup35NM droplet preparation. The droplets were observed via confocal microscopy (LSM 710, Carl Zeiss AG. Jena, Germany) at 100× magnification at an excitation wavelength of 488 nm and a detection wavelength of 493–634 nm. To bleach AF488Sup35 droplets in the region of interest (ROI), 488 and 440 nm laser treatments were applied. When the droplet was partially bleached, the ROI was set as a circle with a radius r = 0.3 μm. The time-lapse of FI, $f(t)$, was fitted to the exponential function $f(t) = A(1-e^{-t/\tau})$ (40) (where A and τ are the arbitrary constant and recovery timescale, respectively), which was used to determine the diffusion coefficient $D \approx r^2 / \tau$.

Measurement of Sup35NM concentration in droplets

A calibration curve was obtained using 0–0.5 μM AF488-tagged Sup35NM with 2% agarose, 10% PEG, 20 μM ThT, 60 mM GdnHCl, 0.1 mM TrisHCl buffer, and 4 mM phosphate buffer. The samples were prepared following the procedure described for Sup35NM droplet preparation. Under these conditions, AF488-tagged Sup35NM did not form droplets. The FI of each sample was measured using confocal microscopy at 100× magnification at an excitation wavelength of 488 nm and a detection wavelength of 493–634 nm. Droplets were prepared in the same manner as that for FRAP measurement, and the FIs of three droplets in different positions were measured. Protein concentration in each droplet was calculated from the calibration curve.

Observation of amyloid formation from Sup35NM droplets

The prepared Sup35NM droplets in agarose gel were observed via confocal microscopy at 20× magnification at an excitation wavelength of 445 nm and a detection wavelength of 454–581 nm. The temperature was controlled at 27 °C using a stage top incubator (INUG2-WSKM-SET; TOKAI HIT, Shizuoka, Japan) at 0.5–1-h intervals. At each time point, 10 *z*-slice images with a 3-μm interval were obtained for 1.19 mm^2 areas. Since the FI of the droplets increased with time, the laser power and gain conditions were adjusted at every time point. At all time points, images were taken with laser power = 1% and gain = 900, which were used for the detection of droplets. In addition, when the FIs of the droplets were saturated, images were taken at lower laser power and gain conditions (typically, laser power = 0.2–1% and gain = 700–900).

Image analysis

The obtained confocal micrographs were analyzed using a Python script developed in-house. Firstly, the droplets were detected using the images obtained at laser power = 1% and gain = 900. In this step, image contrast was increased 5 times, and the threshold of the gray value of droplet detection was 38550 (in a 16-bit gray scale). The FI of each droplet in each *z*-slice image was measured using the lowest gain or laser power condition. Then, the *z* center position of a droplet was determined by finding the *z*-slice image in which the FI of the droplet was the highest. Using this *z*-position, the center position, area, and FI of the droplet were measured under the highest gain/laser condition where the droplet's gray value was not saturated. To extract the droplet from extending amyloid branches, the droplet was defined as the pixels where the FI was higher than half of the average FI of the nine highest pixels in the droplet. The detected droplets were identified by correcting the misregistration of image positions at each time point using the coordinate values of droplet centers. In detail, misregistration was corrected by finding the image position shift where the most coordinate values of the droplet centers match those in the first time point. The time course of FI and the area of each droplet were then obtained. The droplets with more than one nucleation event occurring ("nucleated droplets") were detected using the threshold of FI (Equation 2).

In this method, the droplets sometimes could not be identified even if they existed in the image and had been identified in previous or subsequent measurements because of the slight *z* shift of the measurement or fibril extension, which can change the coordinates of the droplet center. In these cases, we predicted the nucleation of the droplets undetected in the *n*th observation based on the following rules:

1) If the droplet did not nucleate in the (*n*+1)th observation, it did not nucleate in the *n*th observation (Figure S9).
2) If the droplet nucleated in the (*n*-1)th observation, it also nucleated in the *n*th observation (Figure S10).
3) If nucleation of the droplet cannot be determined based on rules (1) and (2), the probability of nucleation in the *n*th observation obtained by fitting of Equation 7 was extrapolated.

The summary of the number of detected droplets is shown in Table S2. Since the identified droplet number decreased with time, only the data in which more than 80% of droplets were identified without rule 3 were used for the fitting of $N_{nucleation}/N_{total}$.

Monitoring of amyloid formation using the conventional plate reader method

To investigate amyloid formation in solution, solutions containing 15–43 μM Sup35NM were prepared with 2% agarose, 20 μM ThT, 60 mM GdnHCl, 0.1 mM TrisHCl buffer, and 4.3 mM phosphate buffer. To monitor the amyloid formation from the Sup35NM droplets, droplets were prepared without agarose in the manner described above. The resulting sample contained 39 μM Sup35NM, 10% PEG, 20 μM ThT, 60 mM GdnHCl, 0.1 mM TrisHCl buffer, and 4.3 mM phosphate buffer. Amyloid formation was monitored by measuring the FI of ThT using a microplate reader (Filter Max F5; Molecular Devices, San Jose, CA, USA) with an excitation wavelength of 413–448 nm and a detection wavelength of 475–495 nm at 27 °C without shaking. The obtained result was analyzed using the global fit of the secondary nucleation model in Amylofit (44), and the obtained kinetic parameters were converted into those of the two-step nucleation model (SI Appendix).

Theoretical analysis of amyloid nucleation rate

The normalized FI, *F*, was calculated in each droplet using the equation below:

$$F = \int \frac{F_{pixel}}{V} dA \quad (1)$$

where F_{pixel}, *A*, and *V* are the FI of one pixel in a droplet, droplet area in the z-slice image closest to the center of the droplet, and droplet volume, respectively. *F* is proportional to ThT concentration when the FI of ThT molecules is the same.

To distinguish nucleated droplets from non-nucleated droplets, we calculated the threshold of F as follows:

$$F_{threshold} = F_{ave} + 5\,F_{\sigma} \quad (2)$$

where F_{ave} and F_{σ} are the average and standard deviation of *F*, respectively, at time *t*.

Next, we investigated amyloid nucleation in the droplets by following the nucleation rate analysis technique in emulsion(36,45,46). Since amyloid nucleation is considered to follow a Poisson distribution, similar to protein crystal nucleation (47, 48), the probability of *m* nucleation events inside a droplet of volume *V* during time *τ* with a nucleation rate of *J* is described as follows:

$$P_m = \frac{(-\lambda)^m}{m!} exp(-\lambda), \lambda = \int_0^{\tau} JV dt \quad (3)$$

where λ is the expected value of the nucleation events in a droplet.

Because the nuclei in a droplet did not exhibit transfer to other droplets (Figure 2D), we assumed that each droplet was independent. Therefore, the time evolution of the measured $N_{nucleation}/N_{total}$

(Figure 3C) can be reproduced by the cumulative distribution function of P_m, with a probability ($P_{\tau,m}$) that *m*th nucleation event within a droplet of volume *V* occurred before τ s elapsed.

$$P_\tau = 1 - \sum_{i=0}^{m-1} \frac{(-\lambda)^i}{i!} exp(-\lambda) \quad (4)$$

Using the two-step nucleation model, which assumes a two-step reaction (25, 26, 35, 36, 37) the nucleation rate *J*(*t*), expressed as m^{-3} s^{-1}, of the initial nucleation events is described as follows:

$$J(t) = k_o k_{conv} {C_{droplet}}^{n_o+n_{conv}} t \quad (5)$$

where k_o is the rate constant of oligomer formation from monomers; k_f is the rate constant of oligomer conversion into fibrils (or nuclei); $C_{droplet}$ is the Sup35NM monomer concentration in droplets; n_o is the reaction order of oligomer formation from monomers; and n_{conv} is the reaction order of oligomer conversion into fibrils (*SI Appendix*).

Combining Equations 3 and 5, $P_{\tau,m}$ in a two-step nucleation model is described as follows:

$$P_{\tau,m} = 1 - \sum_{i=0}^{m-1} \frac{\left(-\frac{V k_o k_{conv} {C_{droplet}}^{n_o+n_{conv}} t^2}{2}\right)^i}{i!} exp\left(-\frac{V k_o k_{conv} {C_{droplet}}^{n_o+n_{conv}} t^2}{2}\right) \quad (6)$$

In particular, when *m* = 1, $P_{\tau,m}$ is described as below:

$$P_{\tau,1} = 1 - exp\left(-V k_o k_{conv} {C_{droplet}}^{n_o+n_{conv}} t^2/2\right) = 1 - exp(-VJt/2) \quad (7)$$

Acknowledgments

This work was supported by Japan Society for the promotion of Science Grant-in-Aid for Scientific Research on Innovative Areas (20H04691); Japan Science and Technology Agency (FOREST, JPMJFR211Y); Naito Science & Engineering Foundation; and the MEXT Program for Supporting Construction of Core Facilities (JPMXS0440600021 and JPMXS0440600022). The authors would like to express sincere gratitude to Prof. Kazumasa Ohashi, Ms. Eiko Hanzawa, Prof. Eriko Nango, and Prof. Takaaki Fujiwara of the Tohoku University for their technical support.

References

1. M. R. Sawaya, M. P. Hughes, J. A. Rodriguez, R. Riek, D. S. Eisenberg, The expanding amyloid family: Structure, stability, function, and pathogenesis. *Cell* 184, 4857–4873 (2021).
2. T. P. J. Knowles, M. Vendruscolo, C. M. Dobson, The amyloid state and its association with protein misfolding diseases. *Nat. Rev. Mol. Cell Biol.* 15, 384–396 (2014).
3. R. Crespo, F. A. Rocha, A. M. Damas, P. M. Martins, A generic crystallization-like model that describes the kinetics of amyloid fibril formation. *J. Biol. Chem.* 287, 30585–30594 (2012).
4. J. T. Jarrett, P. T. Lansbury, Seeding “one-dimensional crystallization” of amyloid: A pathogenic mechanism in Alzheimer’s disease and scrapie? *Cell* 73, 1055–1058 (1993).
5. G. Meisl, *et al.*, Molecular mechanisms of protein aggregation from global fitting of kinetic models. *Nat. Protoc.* 11, 252–272 (2016).
6. Y. Yoshimura, *et al.*, Distinguishing crystal-like amyloid fibrils and glass-like amorphous aggregates from their kinetics of formation. *Proc. Natl. Acad. Sci. U. S. A.* 109, 14446–14451 (2012).
7. S. Ray, *et al.*, α-synuclein aggregation nucleates through liquid–liquid phase separation. *Nat. Chem.* 12, 705–716 (2020).

8. A. Patel, *et al.*, A liquid-to-solid phase transition of the ALS protein FUS accelerated by disease mutation. *Cell* 162, 1066–1077 (2015).
9. S. Ambadipudi, J. Biernat, D. Riedel, E. Mandelkow, M. Zweckstetter, Liquid-liquid phase separation of the microtubule-binding repeats of the Alzheimer-related protein Tau. *Nat. Commun.* 8, 275 (2017).
10. N. M. Kanaan, C. Hamel, T. Grabinski, B. Combs, Liquid–liquid phase separation induces pathogenic tau conformations in vitro. *Nat. Commun.* 11, 2809 (2020).
11. W. M. Babinchak, et al., The role of liquid–liquid phase separation in aggregation of the TDP-43 low-complexity domain. *J of Biol. Chem.* 294, 6306 (2019)
12. N. Sekiyama, *et al.*, ALS mutations in the TIA-1 prion-like domain trigger highly condensed pathogenic structures. *Proc. Natl. Acad. Sci. U. S. A.* 119, e2122523119 (2022).
13. A. Molliex, *et al.*, Phase separation by low complexity domains promotes stress granule assembly and drives pathological fibrillization. *Cell* 163, 123–133 (2015).
14. T. M. Franzmann, *et al.*, Phase separation of a yeast prion protein promotes cellular fitness. *Science* 359 (2018).
15. S. F. Banani, H. O. Lee, A. A. Hyman, M. K. Rosen, Biomolecular condensates: Organizers of cellular biochemistry. *Nat. Rev. Mol. Cell Biol.* 18, 285–298 (2017).
16. S. Boeynaems, *et al.*, Protein phase separation: A new phase in cell biology. *Trends Cell Biol.* 28, 420–435 (2018).
17. W. M. Babinchak, W. K. Surewicz, Liquid–liquid phase separation and its mechanistic role in pathological protein aggregation. *J. Mol. Biol.* 432, 1910–1925 (2020).
18. N. A. Yewdall, A. A. M. André, T. Lu, E. Spruijt, Coacervates as models of membraneless organelles. *Curr. Opin. Colloid Interface Sci.* 52*,* 101416 (2021).
19. W. M. Babinchak, *et al.*, The role of liquid–liquid phase separation in aggregation of the TDP-43 low-complexity domain. *J. Biol. Chem.* 294, 6306–6317 (2019).
20. C. Yuan, *et al.*, Nucleation and growth of amino acid and peptide supramolecular polymers through liquid–liquid phase separation. *Angew. Chem.* 131, 18284–18291 (2019).
21. W. Mori, *et al.*, Differences in interaction lead to the formation of different types of insulin amyloid. *Sci. Rep.* 12, 8556 (2022).
22. L. Guo, *et al.*, Nuclear-import receptors reverse aberrant phase transitions of RNA-binding proteins with prion-like domains. *Cell* 173, 677–692.e20 (2018).
23. Y. Xing, *et al.*, Amyloid aggregation under the lens of liquid−liquid phase separation. *J. Phys. Chem. Lett.* 12, 368–378 (2021).
24. D. Kashchiev, R. Cabriolu, S. Auer, Confounding the paradigm: Peculiarities of amyloid fibril nucleation. *J. Am. Chem. Soc.* 135, 1531–1539 (2013).
25. A. Šarić, Y. C. Chebaro, T. P. J. Knowles, D. Frenkel, Crucial role of nonspecific interactions in amyloid nucleation. *Proc. Natl. Acad. Sci. U. S. A.* 111, 17869–17874 (2014).
26. T. C. T. Michaels, *et al.*, Dynamics of oligomer populations formed during the aggregation of Alzheimer's Aβ42 peptide. *Nat. Chem.* 12, 445–451 (2020).
27. Y. Shin, C. P. Brangwynne, Liquid phase condensation in cell physiology and disease. *Science* 357 (2017).
28. B. Y. Feng, *et al.*, Small-molecule aggregates inhibit amyloid polymerization. *Nat. Chem. Biol.* 4, 197–199 (2008).
29. R. Krishnan, S. L. Lindquist, Structural insights into a yeast prion illuminate nucleation and strain diversity. *Nature* 435, 765–772 (2005).
30. Y. Ohhashi, *et al.*, Molecular basis for diversification of yeast prion strain conformation. *Proc. Natl. Acad. Sci. U. S. A.* 115, 2389–2394 (2018).

31. P. M. Tessier, S. Lindquist, Prion recognition elements govern nucleation, strain specificity and species barriers. *Nature* 447, 556–561 (2007).
32. Y. O. Chernoff, et al., Application of yeast to studying amyloid and prion diseases. *Adv Genet* 105, 293 (2020).
33. J. R. Glover, *et al.*, Self-seeded fibers formed by Sup35, the protein determinant of [PSI+], a heritable prion-like factor of S. cerevisiae. *Cell* 89, 811–819 (1997).
34. M. Mimura, *et al.*, Quadruplex folding promotes the condensation of linker histones and DNAs via liquid–liquid phase separation. *J. Am. Chem. Soc.* 143, 9849–9857 (2021).
35. A. J. Dear, *et al.*, Kinetic diversity of amyloid oligomers. *Proc. Natl. Acad. Sci. U. S. A.* 117, 12087–12094 (2020).
36. D. Kashchiev, P. G. Vekilov, A. B. Kolomeisky, Kinetics of two-step nucleation of crystals. *J. Chem. Phys.* 122, 244706 (2005).
37. D. Gebauer, M. Kellermeier, J. D. Gale, L. Bergström, H. Cölfen, Pre-nucleation clusters as solute precursors in crystallisation. *Chem. Soc. Rev.* 43, 2348–2371 (2014).
38. E. Chatani, *et al.*, Early aggregation preceding the nucleation of insulin amyloid fibrils as monitored by small angle X-ray scattering. *Sci. Rep.* 5, 15485 (2015).
39. A. S. Sawner, *et al.*, Modulating α-synuclein liquid–liquid phase separation. *Biochemistry* 60, 3676–3696 (2021).
40. S. Elbaum-Garfinkle, *et al.*, The disordered P granule protein LAF-1 drives phase separation into droplets with tunable viscosity and dynamics. *Proc. Natl. Acad. Sci. U. S. A.* 112, 7189–7194 (2015).
41. K. F. Kelton, A. L. Greer, *Nucleation in Condensed Matter – Applications in Materials and Biology* (Elsevier, 2010), vol. 15, p. 726.
42. K. Nakajima, et al., Macromolecular crowding and supersaturation protect hemodialysis patients from the onset of dialysis-related amyloidosis. *Nat. Commun.* 13, 1 (2022).
43. A. H. DePace, A. Santoso, P. Hillner, J. S. Weissman, A critical role for amino-terminal glutamine/asparagine repeats in the formation and propagation of a yeast prion. *Cell* 93, 1241–1252 (1998).
44. T. P. J. Knowles, *et al.*, An analytical solution to the kinetics of breakable filament assembly. *Science* 326, 1533–1537 (2009).
45. B. Vonnegut, Variation with temperature of the nucleation rate of supercooled liquid tin and water drops. *J. Colloid Sci.* 3, 563–569 (1948).
46. M. Fukuyama, A. Akiyama, M. Harada, T. Okada, A. Hibara, Microfluidic protein crystallisation controlled using spontaneous emulsification. *Anal. Methods* 7, 7128–7131 (2015).
47. E. Chatani, N. Yamamoto, Recent progress on understanding the mechanisms of amyloid nucleation. *Biophys. Rev.* 10, 527–534 (2018).
48. O. Galkin, P. G. Vekilov, Are nucleation kinetics of protein crystals similar to those of liquid droplets? *J. Am. Chem. Soc.* 122, 156–163 (2000).